Computers and Concrete, Vol. 4, No. 2 (2007) 135-156
DOI: http://dx.doi.org/10.12989/cac.2007.4.2.135

3D nonlinear mixed finite-element analysis of RC beams and plates with and without FRP reinforcement

M. Hoque[†], N. Rattanawangcharoen[‡] and A. H. Shah[‡†]

Department of Civil Engineering, The University of Manitoba, Winnipeg,
Manitoba, Canada R3T 5V6

Y. M. Desai[‡‡]

Department of Civil Engineering, Indian Institute of Technology Powai, Mumbai 400076, India

(Received May 15, 2006, Accepted February 5, 2007)

Abstract. Three 3D nonlinear finite-element models are developed to study the behavior of concrete beams and plates with and without external reinforcement by fibre-reinforced plastic (FRP). All three models are formulated based upon the 3D theory of elasticity. The stress model is modified from the element developed by Ramtekkar, *et al.* (2002) to incorporate material nonlinearity in the formulation. Both transverse stress and displacement components are used as nodal degrees-of-freedom to ensure the continuity of both stress and displacement components between the elements. The displacement model uses only displacement components as nodal degrees-of-freedom. The transition model has both stress and displacement components as nodal degrees-of-freedom on one surface, and only displacement components as nodal degrees-of-freedom on the opposite surface. The transition model serves as a connector between the stress and the displacement models. The developed models are validated by comparing the results of the analyses with an existing experimental result. Parametric studies of the effects of the externally reinforced FRP on the load capacity of reinforced concrete (RC) beams and concrete plates are performed to demonstrate the practicality and the efficiency of the proposed models.

Keywords: 3D nonlinear finite element models; mixed-finite element model; 3D theory of elasticity; nonlinear analysis of RC beams and plates; material nonlinearity; RC beams and plates with and without FRP reinforcement.

1. Introduction

The finite element method has been an important tool in the analysis of both simple concrete structures, such as RC beams, columns, slabs, etc., and complex concrete structures, such as offshore walls, deep beams, shear walls, FRP strengthened RC structures, etc. The development of

---

[†] E-mail: mmhoque2002@yahoo.com
[‡] Assistant Professor, Corresponding Author, E-mail: rattana@cc.umanitoba.ca
[‡†] Professor, E-mail: shah@cc.umanitoba.ca
[‡‡] Professor, E-mail: desai@civil.iitb.ac.in

large memory capacity computers allows engineers and researchers to perform an analysis using finite element with significantly improved accuracy of more complex concrete structures with both material and geometric nonlinearities. A considerable amount of work has been reported in recent literature on the development and application of finite-element models for RC structures, such as the use of separate finite elements for concrete and reinforcement (Kwak and Filippou 1997), finite-element model considering both materials and geometric nonlinearity (Al-Taan and Ezzadeen 1995, Jiang and Mirza 1997, Nitereka and Neale 1999), and finite element with smeared crack model and/ or smeared reinforcement bar model (Vecchio 1989, Hu and Schnobrich 1990, Abbas, *et al.* 2004, and Supaviriyakit, *et al.* 2004).

Vecchio (1989) developed a nonlinear finite element model that included a smeared crack approach to predict the response of RC structures. A secant stiffness approach was used in the model to incorporate the nonlinear constitutive relation for concrete. Polak and Vecchio (1993) modified a finite-element model for the analysis of RC shell structures. In their modified model, a 42 degree of freedom heterosis type degenerate isoparametric quadrilateral element was developed by using a layered-element formulation. Hu and Schnobrich (1990) derived a set of constitutive equations for an incremental finite element analysis, and developed a nonlinear material model for cracked RC structures. The model was able to accurately describe a post-cracking behavior of reinforced concrete. Reinforcement was treated as an equivalent uniaxial layered material placed at the depth of the centerline of the bar. For concrete nonlinear behavior, Saenz's stress-strain curve (Saenz, 1964) was used. The model considered smeared crack representation, rotating crack approach, tension stiffening, the stress-degrading effect of concrete parallel to the crack direction, and shear retention of concrete on the crack surface. Al-Taan and Ezzadeen (1995) developed a numerical procedure based on the finite-element method for geometric and material nonlinear analysis of RC members. A frame element with a composite layer system was used to model the structure. For the nonlinear solution, an incremental-iterative technique based on Newton-Raphson's method was employed. Displacement degrees-of-freedom were approximated with parabolic interpolation functions in the axial direction, and cubic interpolation functions in the other directions. Cerioni and Mingardi (1996) introduced a finite-element model for an analysis of RC foundation plates. In their analysis, the RC plate was modeled with material nonlinear layered finite elements. Jiang and Mirza (1997) developed a rational numerical model for a nonlinear analysis of RC slabs. Material nonlinearities for both concrete and steel were considered. In their model, a RC slab was first divided into a number of composite elements, and each of the composite elements was then assembled into a single concrete plate element and a small number of steel beam elements. Kirchhoff thin plate theory was used in the plate element. Kwak and Filippou (1997) introduced a finite-element model where concrete and reinforcing bars were represented by separate material models. Concrete was modeled by an eight-node element and the reinforcement was modeled by a two-node truss element. A bond link element was used to connect the two elements together. Bhatt and Kader (1998) presented a 2-D parabolic isoparametric quadrilateral finite element based on tangent stiffening method for predicting the shear strength of RC rectangular beams. Kwak and Kim (2002) introduced a new finite-element model for beams based on the moment-curvature relations of RC sections, including the bond-slip and tension softening branch. They used the well-established Timoshenko beam theory in the analysis. Later, Abbas, *et al.* (2004) presented a 3-D nonlinear finite-element model for reinforced concrete structures under impact loading. The reinforcement was smeared as a two dimensional membrane of an equivalent thickness. The layer was assumed to resist only the axial stresses in the direction of the reinforcing bars. Recently, Phuvoravan and

Sotelino (2005) presented a finite element model for a nonlinear analysis of RC slabs that combined a four-node Kirchhoff shell element for concrete with a two-node Euler beam element for the steel reinforcing bars. A rigid link was used to connect these two element types. This model can ensure the exact location of steel reinforcement bars.

Over the last decade, civil engineers have focused their interest on the use of FRP for its superior characteristics over steel reinforcement. A large number of experiments on the topic were done in this time period. Many researchers have also focused on the development of finite-element models for the analysis of FRP reinforced concrete structures. Shahawy, *et al.* (1996) used a 2-dimensional nonlinear finite-element model to analyze beams strengthened with carbon fibre-reinforced plastic (CFRP). Nitereka and Neale (1999) developed a nonlinear finite-element layered model to predict the complete load-deformation response of reinforced concrete beams flexurally strengthened by composite materials. Their model considered both material and geometric nonlinearities. The numerical results confirmed the effectiveness of using externally bonded fiber reinforced composite laminates as a viable technique for strengthening concrete beams in flexure. Ferreira, *et al.* (2001) presented a finite-element model to analyze RC beams with FRP re-bars. The first order shear deformation theory was used in the analysis of concrete shells reinforced with internal composite unidirectional re-bars. The concrete was modeled with smeared crack concepts. A perfect plastic and a strain-hardening plasticity approach were used to model the compressive behavior of the concrete. A dual criterion for yielding and crushing in terms of stresses and strains were considered. For tension in concrete, the influence of the cracked concrete zones on the structural behavior was considered in their study. Supaviriyakit, *et al.* (2004) developed a finite-element model to analyze RC beam strengthened with externally bonded FRP plates. The concrete and reinforcing steel were modeled together by 8-node 2-D isoparametric plane stress RC elements. The RC element considered the effect of cracks and reinforcing steel as being smeared over the entire element. The four-way fixed crack model was used to deal with the cracks in concrete. The FRP plate was modeled as a 2D elasto-brittle element. Hu, *et al.* (2004) incorporated the nonlinear constitutive model for FRP suggested by Hahn and Tsai (1973) to the ABAQUS finite-element program to study the influences of fibre-orientation, beam length, and reinforcement ratios on the ultimate strength of RC beams strengthened by FRP. They concluded that the beams strengthened by FRP at the bottom have higher ultimate strength than the beams strengthened by FRP on the sides.

To the authors' knowledge, no researcher has worked on a 3-D finite-element model for nonlinear analysis of concrete structures using a mixed model approach. In this paper, we present three 3-D layer-wise 18-node finite-element models for nonlinear analysis of concrete structures with and without FRP reinforcement. In the first two models, mixed finite-element formulation based on three-dimensional elasticity theory is employed by approximating displacement components in the form of nodal displacements and nodal stresses. The first model was originally developed by Ramtekkar, *et al.* (2002). In it, both the transverse stress and displacement components are used as nodal degrees-of-freedom. The model was modified in this study to incorporate material nonlinearity, smeared crack concept, and smeared reinforcement. In the second model, three nodal displacement components in the coordinate axis directions and three nodal transverse stress components are used as degrees-of-freedom on one surface while only three nodal displacement components in the coordinate axis directions are used as degrees-of-freedom on the opposite surface. In the third model, three nodal displacement components in the coordinate axis directions are considered as nodal degrees-of-freedom. Local-global phenomena are introduced by considering all three models together. For convenience, the first model, the second model, and the third model will be referred to as the stress, the transition, and the displacement models, respectively. In order to reduce the computational time, a less degree of freedom element, i.e., the displacement model, is used where a compromise in an accuracy of stress calculations is tolerated. A higher degree of freedom element (i.e. the stress model) is used where a higher degree of accuracy in stress calculations is required. The transition model serves as a connector between the zone using the displacement model and that using the stress model. Concrete material nonlinearity is considered using Saenz's stress-strain formulation (Saenz 1964) in the finite-element framework. Steel is considered as a bilinear elasto-plastic material and smeared uniformly over the elements where the steel reinforcement is located. Only unidirectional stress is considered along the reinforcing bars direction. The accuracy is verified by comparing the results of the developed models with the experimental results of an RC beam strengthened with external FRP reinforcement. Numerical examples are provided to illustrate the applicability, efficiency, and suitability of the models.

2. Finite-element models

Three eighteen-node, three-dimensional finite-element models are formulated in this study. The

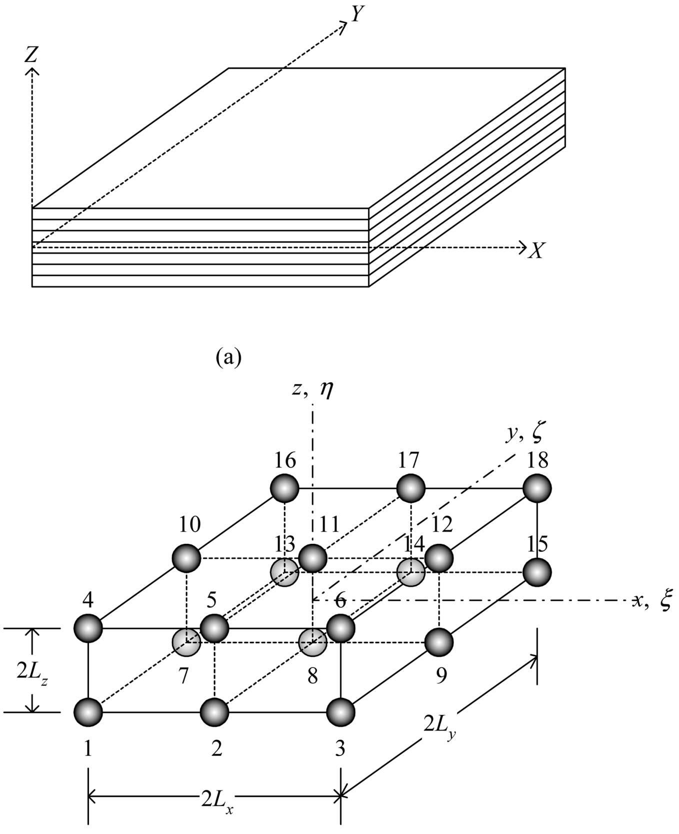

Fig. 1 (a) Laminated plate and global reference axes and (b) Geometry of 18-node finite element and local reference axes stress model for nonlinear analysis is formulated and modified from the mixed finite-element model developed by Ramtekkar, *et al.* (2002). The transition and the displacement models are modified from the stress model. In the development of all three finite-element models in this study, an anisotropic plate consisting of N orthotropic layers shown in Fig. 1(a) is considered. The plate is discretized into a number of 3-D, 18 node elements shown in Fig. 1(b). Each element lies completely within a layer and no element crosses the interface between any two successive layers. The local reference axes are parallel to the global reference axes.

The stress-strain relation for an orthotropic element in *i*th the layer in a material coordinate system is expressed as

$$\begin{Bmatrix} \sigma_1 \\ \sigma_2 \\ \sigma_3 \\ \tau_{12} \\ \tau_{13} \\ \tau_{23} \end{Bmatrix} = \begin{bmatrix} C_{11} & C_{12} & C_{13} & 0 & 0 & 0 \\ & C_{22} & C_{23} & 0 & 0 & 0 \\ & & C_{33} & 0 & 0 & 0 \\ sym. & & & C_{44} & 0 & 0 \\ & & & & C_{55} & 0 \\ & & & & & C_{66} \end{bmatrix} \begin{Bmatrix} \varepsilon_1 \\ \varepsilon_2 \\ \varepsilon_3 \\ \gamma_{12} \\ \gamma_{13} \\ \gamma_{23} \end{Bmatrix} \tag{1}$$

where $\langle \sigma_1\ \sigma_2\ \sigma_3\ \tau_{12}\ \tau_{13}\ \tau_{23} \rangle^T$ is the stress vector and $\langle \varepsilon_1\ \varepsilon_2\ \varepsilon_3\ \gamma_{12}\ \gamma_{13}\ \gamma_{23} \rangle^T$ is the strain vector. $[C]$ is the material constitutive relations. Superscript T denotes matrix transpose. Subscripts 1, 2, and 3 refer to the principal axes of the material. The stress-strain relation for the *i*th layer in the local coordinates x, y, and z is expressed as

$$\{\sigma\} = [D]\{\varepsilon\} \tag{2}$$

Here the stress and the strain vectors with respect to the local coordinates are

$$\begin{aligned} \{\sigma\} &= \langle \sigma_x\ \sigma_y\ \sigma_z\ \tau_{xy}\ \tau_{xz}\ \tau_{yz} \rangle^T \\ \{\varepsilon\} &= \langle \varepsilon_x\ \varepsilon_y\ \varepsilon_z\ \gamma_{xy}\ \gamma_{xz}\ \gamma_{yz} \rangle^T \end{aligned} \tag{3}$$

and

$$[D] = \left[\begin{array}{c:c} D_{ij} & 0 \\ \hdashline 0 & D_{lm} \end{array}\right] \qquad \begin{aligned} i,j &= 1,2,3,4 \\ l,m &= 5,6 \end{aligned} \tag{4}$$

The material constitutive relations for each material will be elaborated in the next section.

2.1. The stress model

Detail of the formulation of the stress model can be found in Ramtekkar, *et al.* (2002). Only brief summary of the formulation will be given here.

The displacement components in the x, y, and z coordinates, $u(x,y,z)$, $v(x, y, z)$ and $w(x, y, z)$, respectively, are approximated by quadratic variations in the plane of the plate and a cubic variation in the transverse direction, and are expressed as

$$u_k(x,y,z) = \sum_{i=1}^{3}\sum_{j=1}^{3} g_i h_j a_{0ijk} + z\sum_{i=1}^{3}\sum_{j=1}^{3} g_i h_j a_{1ijk} + z^2\sum_{i=1}^{3}\sum_{j=1}^{3} g_i h_j a_{2ijk} + z^3\sum_{i=1}^{3}\sum_{j=1}^{3} g_i h_j a_{3ijk}, \qquad k = 1,2,3 \tag{5}$$

where

$$g_1 = \frac{\xi}{2}(\xi - 1),\quad g_2 = 1 - \xi^2,\quad g_3 = \frac{\xi}{2}(1 + \xi),\quad \xi = \frac{x}{L_x} \tag{6}$$

$$h_1 = \frac{\zeta}{2}(\zeta - 1),\quad h_2 = 1 - \zeta^2,\quad h_3 = \frac{\zeta}{2}(1 + \zeta),\quad \zeta = \frac{y}{L_y} \tag{7}$$

Here $u_1(x, y, z) = u$, $u_2(x, y, z) = v$, and $u_3(x, y, z) = w$. The generalized coordinates $a_{mijk}(m=0, 1, 2, 3;$ $i, j, k = 1, 2, 3)$ are functions of z. It is noted that the variation of displacement fields is assumed to be cubic along the z- or the thickness-direction of the element, hence, the transverse stresses τ_{xz}, τ_{yz}, and σ_{zz} can directly be incorporated as nodal degrees-of-freedom. This ensures parabolic variation of transverse stresses in the thickness-direction.

The constitutive relation, Eq. (2), and the strain-displacement relation provide the following equations

$$\begin{aligned}
\frac{\partial u}{\partial z} &= \frac{1}{\Delta}[D_{66}\tau_{xz} - D_{56}\tau_{yz}] - \frac{\partial w}{\partial x} \\
\frac{\partial v}{\partial z} &= -\frac{1}{\Delta}[D_{56}\tau_{xz} - D_{55}\tau_{yz}] - \frac{\partial w}{\partial y} \\
\frac{\partial w}{\partial z} &= \frac{1}{D_{33}}\left[\sigma_z - D_{13}\frac{\partial u}{\partial x} - D_{23}\frac{\partial v}{\partial y} - D_{34}\left(\frac{\partial u}{\partial y} + \frac{\partial v}{\partial x}\right)\right]
\end{aligned} \tag{8}$$

where

$$\Delta = D_{55}D_{66} - D_{56}^2 \tag{9}$$

The displacement fields $u\,(x, y, z)$, $v\,(x, y, z)$ and $w\,(x, y, z)$expressed in Eq. (5), can now be further expressed in terms of nodal variables by using Eqs. (8) as

$$\{u\} = [N]\{q\} \tag{10}$$

where

$$\{u\} = \langle u \quad v \quad w \rangle^T \tag{11}$$

$$\{q\} = \langle \underset{\sim}{q}_1^T\ \underset{\sim}{q}_2^T\ \ldots\ \underset{\sim}{q}_n^T\ \ldots\ \underset{\sim}{q}_{18}^T \rangle^T \tag{12}$$

and

$$\{q_n\} = \langle u_n\ \ v_n\ \ w_n\ \ (\tau_{xz})_n\ \ (\tau_{zy})_n\ \ (\sigma_z)_n \rangle^T \tag{13}$$

The shape function matrix $[N]$ is given in Eqn. (A-1) in the Appendix.

The total potential energy Π of the layer is

$$\Pi = \frac{1}{2}\int_V \{\varepsilon\}^T\{\sigma\}dV - \int_V \{q\}^T\{p_b\}dV - \int_\Sigma \{q\}^T\{P_t\}dS \tag{14}$$

where $\{\, p_b \,\}$ is the body force vector per unit volume and $\{\, p_t \,\}$ is the traction load vector acting on any surface of the composite plate. Here Σ is a surface of the element subjected to traction forces. The strain vector $\{\, \varepsilon \,\}$ and the stress vector $\{\, \sigma \,\}$ can be expressed in terms of nodal degree of freedom as, respectively,

$$\{\varepsilon\} = [B][q] \tag{15}$$

$$\{\sigma\} = [D][B]\{q\} \tag{16}$$

The matrix $[\,B\,]$ is given in Eq. (A-7) in the Appendix.

Minimization of the total potential energy functional, Eq. (14), yields the element property matrix $[\,k\,]^e$ and the element influence vector $\{\,f\,\}^e$, respectively, as

$$[k]^e = \int_{-L_X}^{L_X}\int_{-L_Y}^{L_Y}\int_{-L_Z}^{L_Z}[B]^T[D][B]dxdydz \tag{17}$$

$$\{f\}^e = \int_{-L_X}^{L_X}\int_{-L_Y}^{L_Y}\int_{-L_Z}^{L_Z}[N]^T\{p_b\}dxdydz + \iint_{\Sigma}[N]^T\{p_t\}ds \tag{18}$$

The global equation can be obtained, after the conventional assembly process, in the following form

$$[K]\{Q\} = \{F\} \tag{19}$$

Here $[\,K\,]$, $\{\,Q\,\}$, and $\{\,F\,\}$ are the global property matrix, the global degree of freedom vector, and the global influence vector, respectively.

2.2. Transition model

As mentioned, the transition model is developed as a means to connect the stress and the displacement models. The nodes on one of the surfaces of the element will therefore contain both transverse stresses and displacements as degrees-of-freedom, while the nodes on the opposite surface of the element will only contain displacements as degrees-of-freedom. In order to achieve the aforementioned requirement, the displacement fields in Eq. (5) are modified to be in the form of

$$u_k(x,y,z) = \sum_{i=1}^{3}\sum_{j=1}^{3}g_ih_ja_{0ijk} + z\sum_{i=1}^{3}\sum_{j=1}^{3}g_ih_ja_{1ijk} + z^2\sum_{i=1}^{3}\sum_{j=1}^{3}g_ih_ja_{2ijk} \qquad k = 1,2,3 \tag{20}$$

Assuming the upper surface nodes contain both transverse stresses and displacements as degrees-of-freedom and following a similar derivation as in the stress model, the same form of global equilibrium equation, Eq. (19), is obtained. The only differences here are the nodal degree of freedom vector $\{\,q_n\,\}$ and the shape function matrix $[\,N\,]$ in Eqs. (10) and (13). Here $\{\,q_n\,\}$ is

$$\{q_n\} = \begin{cases} \langle u_n \;\; v_n \;\; w_n\rangle^T & n = m,\ldots,m+2;\; m = 1,7,13 \\ \langle u_n \;\; v_n \;\; w_n \;\; (\tau_{xz})_n \;\; (\tau_{yz})_n \;\; (\sigma_z)_n\rangle^T & n = m+3,\ldots,m+5;\; m = 1,7,13 \end{cases} \tag{21}$$

The shape function matrix $[\,N\,]$ is given in Eqs. (A-10) and (A-11) in the Appendix.

2.3. Displacement model

The nodal degrees-of-freedom of the displacement model are only displacements x, y, in z directions. Here the displacement fields in Eq. (20) are modified further to be in the form of

$$u_k(x,\,y,\,z)=\sum_{i=1}^{3}\sum_{j=1}^{3}g_ih_ja_{0ijk}+z\sum_{i=1}^{3}\sum_{j=1}^{3}g_ih_ja_{1ijk}\qquad k=1,2,3 \tag{22}$$

The nodal degrees-of-freedom vector $\{q_n\}$ in Eq. (21) becomes

$$\{q_n\}=\langle u_n\ \ v_n\ \ w_n\rangle^T \tag{23}$$

The approximate displacements are expressed in terms of nodal degrees-of-freedom as in Eq. (10). The shape function matrix $[N]$ is given in Eq. (A-10) in the Appendix.

3. Material constitutive relations

3.1. Concrete

For compression, widely accepted Saenz's uniaxial stress-strain (σ–ε) relationship (Saenz 1964) is used in this study. It has the following form:

$$\sigma=\frac{E_c\varepsilon}{1+R_3\dfrac{\varepsilon}{\varepsilon_0}-R_2\left(\dfrac{\varepsilon}{\varepsilon_0}\right)^2+R_1\left(\dfrac{\varepsilon}{\varepsilon_0}\right)^3} \tag{24}$$

where

$$R_1=\frac{R_E(R_f-1)}{(R_\varepsilon-1)^2}-\frac{1}{R_\varepsilon},\ R_2=2R_1-1,\ R_3=R_1+R_E-2 \tag{25}$$

E_c is the initial tangent modulus of concrete, ε_0 is the strain in concrete at the characteristic compressive stress, f_c'. The modular ratio R_E, stress ratio R_f, and strain ratio R_ε are defined as, respectively,

$$R_E=\frac{E_c}{E_0},\ R_f=\frac{f_c'}{f_f},\ R_\varepsilon=\frac{\varepsilon_f}{\varepsilon_0} \tag{26}$$

E_0 is a secant modulus of concrete and ε_f is the strain in concrete at the compressive failure stress, f_f. The tangent modulus of concrete, E_T, corresponding to a specified strain can be found by taking derivatives of the Eq. (24) with respect to strain component. This leads to

$$E_T=\frac{d\sigma}{d\varepsilon}=\frac{E_c\left[1+R_2\left(\dfrac{\varepsilon}{\varepsilon_0}\right)^2-2R_1\left(\dfrac{\varepsilon}{\varepsilon_0}\right)^3\right]}{\left[1+R_3\dfrac{\varepsilon}{\varepsilon_0}-R_2\left(\dfrac{\varepsilon}{\varepsilon_0}\right)^2+R_1\left(\dfrac{\varepsilon}{\varepsilon_0}\right)^3\right]^2} \tag{27}$$

Beyond the peak stress point in the strain-softening region, with further straining, the compressive stress begins to decrease and the equivalent uniaxial tangent modulus becomes negative. In order to circumvent numerical difficulties associated with a negative tangent modulus, once the ultimate yield stress f_c' has been reached, E_T is set to zero and the concrete behaves like perfectly plastic material as shown in Fig. 2. This plastic response is allowed to propagate through an incremental strain $\Delta\varepsilon$, at which time the unbalanced stress is released. This process proceeds in a stepwise

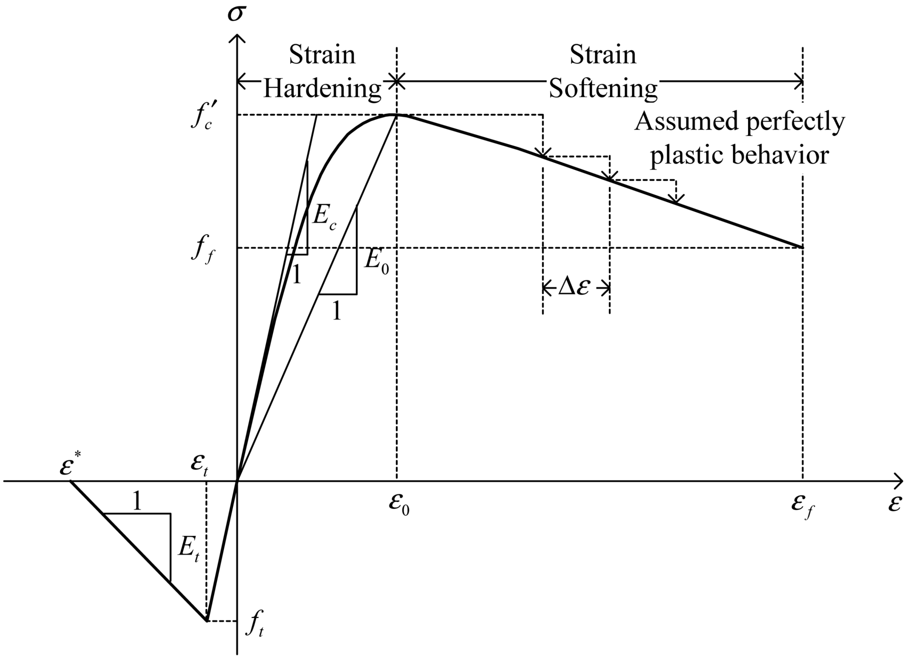

Fig. 2 Uniaxial stress-strain curve for concrete

fashion.

Tangent modulus $E_{pi}(i = 1, 2, 3)$, along the three principle directions can be calculated from the Eq. (24) with the use of the three principal strains from the last load step. The three-dimensional stress and strain can be computed from the following incremental stress-strain relations along the principal direction:

$$\{\Delta\sigma\} = [C^c]\{\Delta\varepsilon\} \tag{28}$$

where $\{\sigma\}$ and $\{\varepsilon\}$ are stress and strain vectors along the principal directions respectively. The symmetric constitutive matrix $[C^c]$ is

$$[C^c] = \begin{bmatrix} \lambda_{p1} & \nu E_{12} & \nu E_{13} & 0 & 0 & 0 \\ \nu E_{12} & \lambda_{p2} & \nu E_{23} & 0 & 0 & 0 \\ \nu E_{13} & \nu E_{23} & \lambda_{p3} & 0 & 0 & 0 \\ 0 & 0 & 0 & \mu_{12} & 0 & 0 \\ 0 & 0 & 0 & 0 & \mu_{13} & 0 \\ 0 & 0 & 0 & 0 & 0 & \mu_{23} \end{bmatrix} \tag{29}$$

where

$$\lambda_{pi}=\frac{(1-\nu)E_{pi}}{(1+\nu)(1-2\nu)}$$

$$\mu_{ij}=\frac{E_{ij}}{2(1+\nu)} \qquad i=1,2;\ j=2,3;\ i\neq j \tag{30}$$

$$E_{ij}=\frac{|\sigma_{pi}|E_{pi}+|\sigma_{pj}|E_{pj}}{|\sigma_{pi}|+|\sigma_{pj}|}$$

In the above equation, σ_{pi} (i=1, 2, 3) are the principal stresses. This constitutive matrix along the principal directions can be transformed to the global direction by applying coordinate transformation.

For tension, initial tangent modulus of concrete E_c is used to find the maximum positive (tensile) stress until crack. After cracking in the concrete takes place, a smeared model is used to represent the discontinuous macro crack behavior. This cracked concrete can still carry some tensile stress perpendicular to the crack, which is termed tension stiffening. In this study, a simple descending line is used to model this tension stiffening phenomenon as shown in Fig. 2. The default value of the strain ε^* at which the tension stiffening stress reduced to zero is $\varepsilon^*=0.001$. In Fig. 2, E_c and E_t are the moduli of elasticity of tensile concrete between zero to fracture strain and from fracture strain to ε^*, respectively. f_t is the maximum stress at fracture of concrete, which has corresponding strain ε_t.

A crack occurs in concrete when the tensile stress in a principal direction exceeds the tensile strength, f_t, of concrete. For this reason, the constitutive matrix, Eq. (29), needs to be modified. After the crack forms, the normal as well as the shear stiffness are reduced. If the failure occurs in the first principal direction (σ_{p1} exceeds f_t) then the modified constitutive matrix $[C^c]$ is

$$[C^c]=\begin{bmatrix} E_0\eta & 0 & 0 & 0 & 0 & 0\\ 0 & \frac{E_{p2}}{1-\nu^2} & \frac{\nu E_{23}}{1-\nu^2} & 0 & 0 & 0\\ 0 & \frac{\nu E_{32}}{1-\nu^2} & \frac{E_{p3}}{1-\nu^2} & 0 & 0 & 0\\ 0 & 0 & 0 & \frac{E_0\eta_S}{2(1+\nu)} & 0 & 0\\ 0 & 0 & 0 & 0 & \frac{E_0\eta_S}{2(1+\nu)} & 0\\ 0 & 0 & 0 & 0 & 0 & \frac{E_{23}}{2(1+\nu)} \end{bmatrix} \tag{31}$$

The constant η in Eq. (31) is the reduction factor of the stiffness normal to the tensile failure plane, and η_S is the reduction factor of the shear stiffness in the tensile failure plane.

When the tensile failure occurs along first and second principal directions, further modification is applied to the constitutive matrix. The new constitutive matrix $[C^c]$ is

$$[C^c] = \begin{bmatrix} E_0\eta & 0 & 0 & 0 & 0 & 0 \\ 0 & E_0\eta & 0 & 0 & 0 & 0 \\ 0 & 0 & \dfrac{E_{p3}}{1-\nu^2} & 0 & 0 & 0 \\ 0 & 0 & 0 & \dfrac{E_0\eta_S}{2(1+\nu)} & 0 & 0 \\ 0 & 0 & 0 & 0 & \dfrac{E_0\eta_S}{2(1+\nu)} & 0 \\ 0 & 0 & 0 & 0 & 0 & \dfrac{E_0\eta}{2(1+\nu)} \end{bmatrix} \tag{32}$$

3.2. Reinforcing steel and smeared model

The stress-strain curve of the reinforcing bar is assumed to be bi-linear, that is, linear elastic up to the steel yield stress (f_y), with a slope of the modulus of elasticity of steel, E_s^r. This is followed by a linear hardening with a slope of the strain hardening modulus, E_T^r up to the steel ultimate strength (f_u). The uni-directional constitutive matrix for steel $[D^r]$ contains only the D_{11}^r term, which is equal to either E_s^r or E_T^r, depending on the strain in steel reinforcement. For simplicity, the constitutive relation for concrete used in the smeared element is assumed to be isotropic elastic and the constitutive matrix is $[D^c]$. The constitutive matrix for the smeared model, considering contribution of both concrete and reinforcing steel, is obtained from

$$[D] = (1-V^R)[D^c] + V^R[D^r] \tag{33}$$

Here V^R is the ratio of volume of reinforcement to the total volume of smeared element.

3.3. Fibre-reinforced plastic

The behavior of FRP materials is linear elastic to failure. Ultimate elongation strains are considerably higher than steel yielding strains. This results in ultimate tensile strengths that are typically between four to nine times the yield stress of steel. Failure is sudden and brittle with no load carrying capacity after failure. Mechanical properties of the composites vary to a high degree depending on the orientation of load with respect to the fiber orientation, and the fiber-to-resin volume ratio. FRP materials exhibit the highest strength when loaded in the direction of the fibers, and have only the strength of the resin when loaded perpendicular to the fibers. Generally laminated FRP sheets are used for external reinforcement. The stress-strain relations of FRP for each layer or lamina in three dimensions can be obtained from any mechanics of composite materials textbook, e.g., Gibson (1994).

4. Numerical results and discussion

In all examples, a reinforced FRP is considered to be perfectly bonded to an RC member. No weak interface, de-bonding or delamination is considered in this study. It should be mentioned here that the stress model, however, can simply be modified to incorporate weak interface and first-ply failure of the FRP since the transverse stresses are nodal variables (Ramtekkar, *et al.* 2004, Rattanawangcharoen 2005, 2006).

4.1. Validation of numerical results

In order to verify the numerical results from the present finite-element models, analysis of a simply supported reinforced concrete beam strengthened by FRP at the bottom and subjected to four-point loading, is compared against experimental work done by Shahawy, *et al.* (1996). The geometric properties of the beam are presented in Fig. 3. The mesh used for the beam is shown in Fig. 4.

The material properties of concrete, reinforcing steel, and FRP reinforcement are, respectively, (Shahawy, *et al.* 1996, Hu, *et al.* 2004).

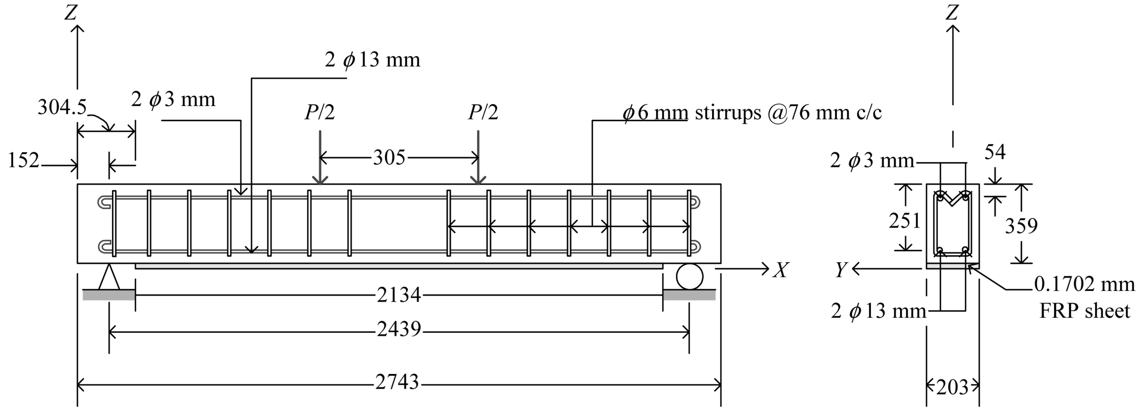

Fig. 3 Geometry of a simply-supported beam under four-point load test (all dimensions are in mm)

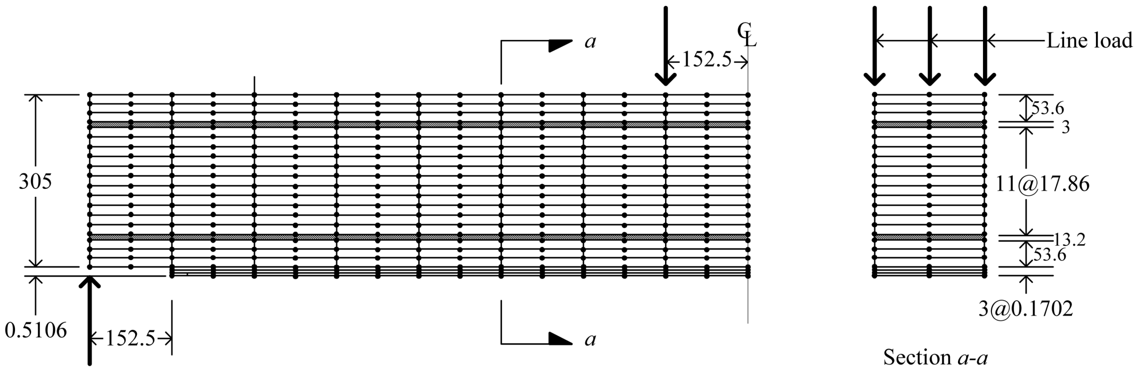

(a) (b)

Fig. 4 Finite-element mesh used for a simply-supported beam under four-point load test (all dimensions are in mm)

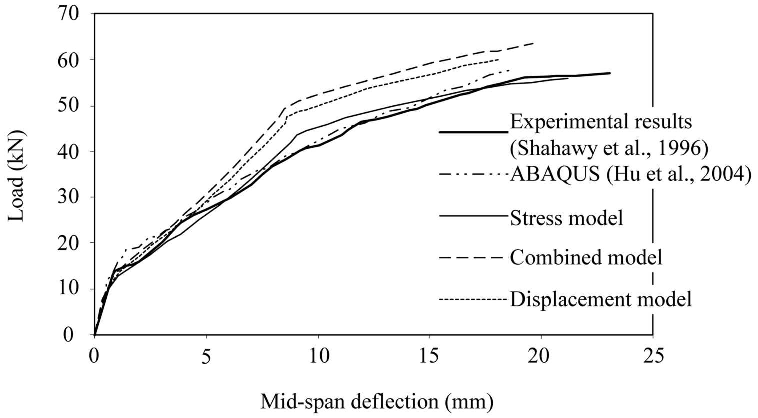

Fig. 5 Load-deflection curves of simply-supported beam under four-point load

$$\begin{array}{llll} \varepsilon_0 = 0.0025 & \varepsilon_f = 0.0035 & f'_c = 41.37 \text{ MPa} & f_f = 10.34 \text{ MPa} \\ f_t = 0.33\sqrt{f'_c} \text{ MPa} & E_c = 4700\sqrt{f'_c} \text{ MPa} & \nu = 0.1 & \eta = 1.0\times10^{-4} \end{array} \tag{34}$$

$$E_s = 199.9 \text{ GPa} \tag{35}$$

$$\begin{array}{ll} E_{11} = 141.3 \text{ GPa} & E_{22} = 14.5 \text{ GPa} \\ G_{12} = G_{13} = 5.86 \text{ GPa} & G_{23} = 3.52 \text{ GPa} \\ \nu_{12} = 0.21 & \end{array} \tag{36}$$

Due to symmetry in the X-direction, only half of the beam was analyzed with a total of 176 elements. Symmetric boundary conditions used are presented in Table 1.

Fig. 5 illustrates the load-deflection curves of the beam obtained from both experimental testing and from the presented finite-element models. Here the combined model consists of the stress model in the outer region, the displacement model in the inner region, and the transition model connecting the two regions. The stress model predicts the ultimate load and the mid-span deflection to differ by 3.6% and 3.8% of the experimental results, respectively. The combined model results differ by 12.3% and 13.0% of the experimental results for the load and the deflection predictions, respectively. The displacement model predicts the load and the deflection to differ by 5.3% and 14.8% of the experimental results, respectively. Therefore, the stress model, when compared to the results from the experiment, provides a very accurate prediction of the mid-span deflection and the ultimate load. It was expected that the combined model would predict both the beam's maximum

Table 1 Boundary conditions used in the analysis of reinforced concrete beam

$X = 0$	$v = w = 0$
$X = L/2$[1]	$u = \tau_{xz} = 0$
$Y = \pm\ b/2$(side surfaces)	$\tau_{xz} = 0$
$Z = d/2$[1](top surface)	$\sigma_z = -P(X, Y);\ \tau_{xz} = \tau_{yz} = 0$
$Z = -d/2$[1] (bottom surface)	$\sigma_z = \tau_{xz} = \tau_{yz} = 0$

[1] L is the span length, b is the width of the section, and d is the depth of the beam.

load and deflection more accurately than the displacement model. However, it was found that it does not give a better prediction of the beam ultimate load, but it does predict the mid-span deflection more accurately.

For comparison purposes, results from ABAQUS (Hu, *et al.* 2004) are also presented in the Figure. The predicted ultimate load was reported to be 0.8% with the predicted maximum mid-span deflection to be 18.7% in comparison to the experimental measurements. It should be noted that in their paper a total of 78 eight-node solid elements were used to model ¼ of the RC beam while in this paper 152 elements are used to model ½ of the RC beam. The nonlinear in-plane shear behaviour of FRP was considered in their paper but is not included in this model.

Two advantages of the proposed stress model over the ABAQUS are 1) to obtain a considerable good result of analysis, only a smear technique is used to model steel reinforcement here instead of rigorously model reinforcement as an actual configuration and 2) the stress model can easily be modified to incorporate weak interface and first-ply failure of FRP as mentioned earlier.

4.2. RC beam with varying number of FRP layers

In this example, the effect that the different number of externally reinforced FRP laminas has on the nonlinear response of a simply supported RC beam is studied. The beam's geometric and mechanical properties are given in Fig. 3 and Eqs. (34)-(36), respectively. The ultimate load ratio (P_u/P_{u0}) and the maximum mid-span deflection ratio (δ_u/δ_{u0}) of the beam without FRP, and with between one and ten layers of FRP are presented in Fig. 6. Here P_u and P_{u0} are the ultimate load of the beam with and without the FRP reinforcement, respectively, whereas δ_u and δ_{u0} are the maximum mid-span deflection of the beam with and without the FRP reinforcement, respectively. It can be seen that increasing the number of layers of FRP increases the load capacity of the beam and reduces the beam's maximum mid-span deflection. The rate increase in the ultimate load is almost constant with the increase in the number of FRP laminas. A slight increase in the maximum mid-span deflection is first noticed when the beam is reinforced with one and two layers of FRP. With more layers of FRP, the maximum mid-span deflection of the beam decreases in an almost linear

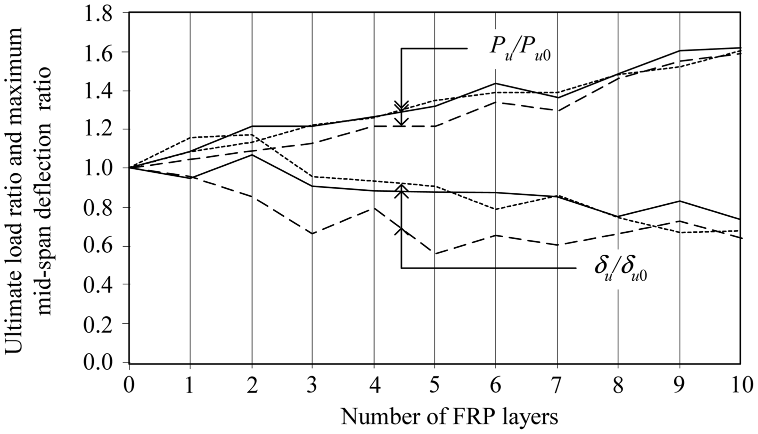

Fig. 6 Ultimate load ratio and maximum mid-span deflection ratio of a simply-supported beam with and without externally reinforced FRP laminates (Solid lines – stress model, Dash lines --- combined model, Dotted lines ---- displacement model)

relation with the number of the FRP reinforcement. The prediction of the ultimate load capacity of the beams is not significantly affected by the use of a different model while the maximum mid-span deflection prediction is. It should be noted that only up to ten layers of FRP is considered here, and that the first-ply failure of the FRP and the delamination between the laminas are both not taken into account in this study.

4.3. RC beam with varying length of FRP reinforcement

The effects of the externally reinforced FRP lengths on the ultimate load and the maximum mid-span deflection of a simply supported RC beam are examined. The beam's geometric and material properties are the same as in the previous example. The beam is reinforced with three layers of FRP. The length of FRP reinforcement varies from zero to one hundred percent of the beam length, no reinforcement and full length reinforcement, respectively. The plots of the ultimate load ratio and the maximum mid-span deflection ratio are in Fig. 7. An increase in the length of the FRP laminates increases the ultimate load of the beam and slightly reduces the maximum mid-span deflection of the beam. The increase in the length of FRP beyond 50% of the beam length, however, does not significantly contribute to the beam bending capacity nor does it affect the maximum mid-span deflection. The displacement model produces an odd prediction of the maximum mid-span deflection when the length of FRP is longer than 50% of the beam length.

4.4. Concrete plate with different lamina scheme of FRP layers

Fibre-orientation angle plays an important role in the increase of the plate strength. This is due to FRP having high strength in the fibre-direction, and low strength in the direction perpendicular to the fibres. To maximize the FRP reinforcement strength, balanced laminate is commonly used. In this example, the effects of a fibre-orientation angle on the ultimate load and on the maximum mid-span deflection of a simply supported on all sides 1000×1000×100 mm concrete plate with external

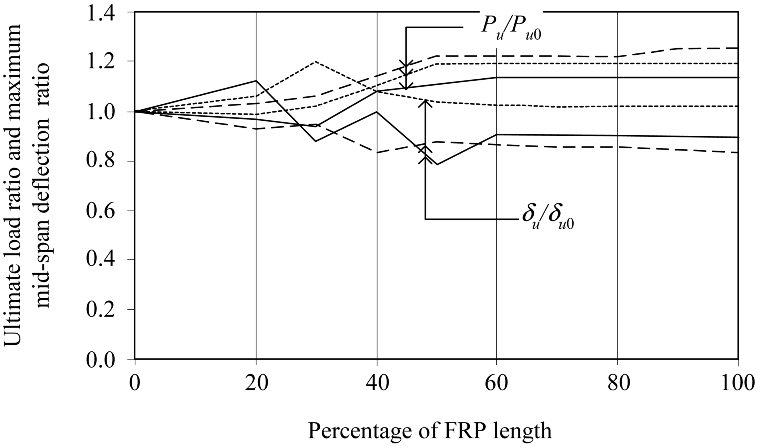

Fig. 7 Ultimate load ratio and maximum mid-span deflection ratio of a simply-supported beam with externally reinforced FRP laminates having different lengths (Solid lines – stress model, Dash lines --- combined model, Dotted lines ---- displacement model)

Table 2 Boundary conditions used in the analysis of the concrete plate

$X = 0$	$v = w = 0$
$X = a/2$[1]	$u = \tau_{xz} = 0$
$Y = 0$	$u = w = 0$
$Y = b/2$[1] (side surface)	$v = \tau_{yz} = 0$
$Z = t/2$[1] (top surface)	$\sigma_z = -P(X, Y)$; $\tau_{xz} = \tau_{yz} = 0$
$Z = -t/2$[1] (bottom surface)	$\sigma_z = \tau_{xz} = \tau_{yz} = 0$

[1] a is the length in the X-direction, b is the width in the Y-direction, and t is the thickness of the plate.

FRP reinforcement on the bottom surface and subjected to a uniformly distributed load on the top are examined. The concrete and FRP properties are, respectively,

$$\begin{array}{llll} \varepsilon_0 = 0.002 & \varepsilon_f = 0.003 & f'_c = 46.1 \text{ MPa} & f_f = 41.5 \text{ MPa} \\ f_t = 3.9 \text{ MPa} & E_c = 43090 \text{ MPa} & \nu = 0.1 & \eta = 1.0\times 10^{-4} \end{array} \tag{37}$$

$$\begin{array}{lll} E_{11} = 138 \text{ GPa} & E_{22} = 14.5 \text{ GPa} & \nu_{12} = 0.21 \\ G_{12} = G_{13} = 5.86 \text{ GPa} & G_{23} = 3.52 \text{ GPa} & \end{array} \tag{38}$$

Due to the bi-axial symmetric property of the problem, only a quarter of the plate is analyzed. The boundary conditions of the plate are given in Table 2. Sixteen-ply $[\beta]_4/[-\beta]_4/[\beta]_4/[-\beta]_4$ FRP, where the fibre-orientation angle β is measured from the longitudinal axis of the plate, is considered. Each ply is 0.17 mm thick. Fig. 8 demonstrates the effects of fibre-orientation angles on the plate's ultimate capacity ratio and the plate's maximum mid-span deflection ratio. Here, the P_{u0} and δ_{u0} are the ultimate load capacity and the maximum deflection at the middle of the cross-ply plate with $[0^\circ]_4/[90^\circ]_4/[0^\circ]_4/[90^\circ]_4$ FRP reinforcement, respectively. The two models, the stress model and the combined model, show that an increase in a fibre-orientation angle increases the

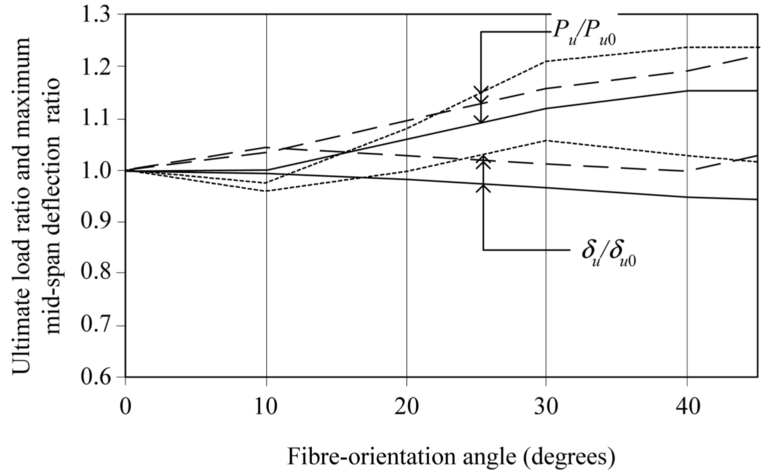

Fig. 8 Ultimate load ratio and maximum deflection ratio of a simply-supported plate with externally reinforced FRP laminates having different fibre-orientation angles of (Solid lines – stress model, Dash lines --- combined model, Dotted lines ---- displacement model)

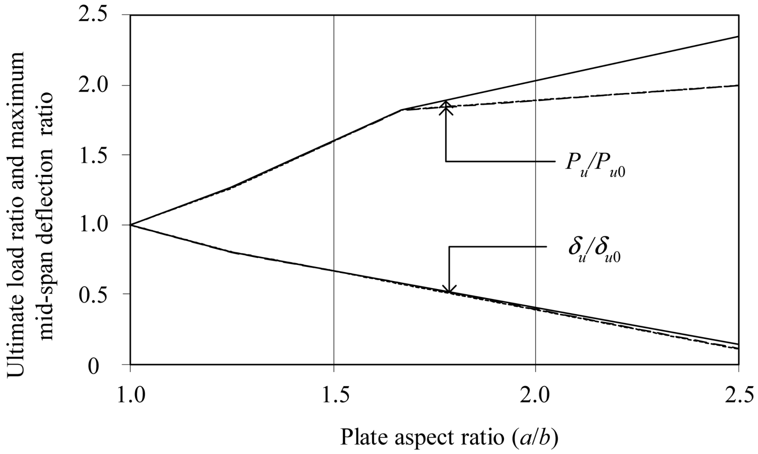

Fig. 9 Ultimate load ratio and maximum deflection ratio of a simply-supported plate with externally reinforced FRP laminates having different aspect ratios (Solid lines – stress model, Dash lines --- combined model, Dotted lines ----· displacement model)

ultimate load capacity of the plate and simultaneously reduces the maximum deflection at the middle of the plate. The displacement model, however, produces questionable results, those being that the ultimate load capacity and the maximum deflection at the middle of the plate both increase with an increase in the fibre-orientation angle. It should be noted here that, due to symmetry, when β is greater than 45°, load-deflection curves of the plate are the same as those when β is less than 45°. The maximum ultimate load is obtained when the fibre-orientation angle reaches 45°. This was expected because of the symmetric property of the problem.

4.5. Externally FRP reinforced concrete plate with different aspect ratios

The effects of the plate aspect (a/b) ratio on the response of a simply supported on all sides FRP reinforced steel-free concrete rectangular plate subjected to a uniformly distributed load are investigated. The geometry of the plate is $a(1000)\times b(1000)\times 100$ mm. The material properties of concrete and FRP are given in Eqns. (37) and (38), respectively. The plate is reinforced on the bottom surface with three layers [0°/90°/0°] FRP. The boundary conditions of the plate are given in Table 2. Fig. 9 illustrates the plate's ultimate capacity ratio and the plate's maximum deflection ratio, both of which were calculated using all three models. The reference ultimate load P_{u0} and the reference maximum deflection δ_{u0} are the values of the plate with $a/b=1$. An increase in the aspect ratio increases the plate's capacity and decreases the plate's maximum deflection. This is expected because the support conditions are all simple supports. When the width of the plate is smaller in comparison to the length, the middle layer of FRP oriented in the width direction helps transferring the load to the width sides. All three models predict the same behaviour and the results are almost identical, with the exception of the plate having large aspect ratios where the stress model provides higher prediction of the plate's capacity.

5. Conclusions

Three 3D nonlinear finite-element models, namely the stress model, the transition model, and the displacement model, were developed to study the behavior of concrete beams and plates with and without external reinforcement of FRP. The stress model uses both transverse stress and displacement components as nodal degrees-of-freedom. The transition model has both stress and displacement components as nodal degrees-of-freedom on one surface, and only displacement components as nodal degrees-of-freedom on the opposite surface. The displacement model uses only displacement components as nodal degrees-of-freedom. The stress model consumes more computational time in the analysis than the displacement model. The displacement model provides less accurate results in stress calculation than the stress model does. The transition model is used to connect the stress and the displacement models, and the resulting model is a combined model. To analyse a beam or plate having a general configuration, the combined model may be used with the stress model in a restricted geometric portion and the displacement model in a general geometric portion. The results of the analysis show that the stress model provides an excellent prediction of the behaviour of an RC beam. Both the displacement and the combined models give higher load capacity and lower maximum displacement. Compared to the displacement model, the combined model does not provide a better prediction of the beam's ultimate load. However, it predicts the mid-span deflection more accurately. All the developed models are used in the study of the nonlinear behaviour of RC beams and concrete plates, with and without external FRP reinforcement. The analyses show that

- An increase in the FRP layers almost linearly increases the load capacity of the RC beams and decreases the maximum mid-span deflection of the beams. This occurs at a higher rate when fewer FRP layers are used and at a lower rate when a larger number of FRP layers are used.
- An increase in the length of FRP reinforcement increases the load capacity of the RC beams and decreases the maximum mid-span deflection of the beams. These effects, however, diminish when the length of FRP reinforcement is greater than 50% of the beam's length.
- The laminating scheme plays an important role in the behaviour of concrete plates. For square plates, it is found that, for sixteen layers of externally reinforced FRP, the fibre-orientation of $[+45^\circ]_4/[-45^\circ]_4/[+45^\circ]_4/[-45^\circ]_4$ provides the highest load capacity and the least maximum deflection of the plates.
- For rectangular concrete plates having different width-to-length ratios with $0^\circ/90^\circ/0^\circ$ FRP reinforcement, an increase in the plate aspect ratio increases the plate capacity and reduces the plate maximum deflection.

Acknowledgements

The work of this study is sponsored by the NSERC, Canada, Discovery Grant RGPIN 261642 and the University of Manitoba. The authors would like to thank Mr. Ward and Mr. Dickinson. Reviewers' comments were greatly appreciated.

Appendix

The shape function matrix in $[N]$ Eq. (10) is given by

$$[N] = [\underline{N}_1 \;\; \underline{N}_2 \;\; \cdots \;\; \underline{N}_n \;\; \cdots \;\; \underline{N}_{18}] \tag{A-1}$$

$$[\underline{N}_n] = \left[\begin{array}{c:c:c:c:c:c} g_i h_j f_q & 0 & -g'_i h_j f_p & \frac{D_{66}}{\Delta} g_i h_j f_p & -\frac{D_{56}}{\Delta} g_i h_j f_p & 0 \\ \hdashline 0 & g_i h_j f_q & -g_i h^*_j f_p & -\frac{D_{56}}{\Delta} g_i h_j f_p & \frac{D_{55}}{\Delta} g_i h_j f_p & 0 \\ \hdashline \begin{matrix} -\frac{D_{13}}{D_{33}} g'_i h_j f_p \\ -\frac{D_{34}}{D_{33}} g_i h^*_j f_p \end{matrix} & \begin{matrix} -\frac{D_{34}}{D_{33}} g'_i h_j f_p \\ -\frac{D_{23}}{D_{33}} g_i h^*_j f_p \end{matrix} & g_i h_j f_q & 0 & 0 & \frac{1}{D_{33}} g_i h_j f_p \end{array}\right] \tag{A-2}$$

$$i = \begin{cases} 1 & \text{for } n = 1,4,7,10,13,16 \\ 2 & \text{for } n = 2,5,8,11,14,17 \\ 3 & \text{for } n = 3,6,9,12,15,18 \end{cases} \qquad j = \begin{cases} 1 & \text{for } n = 1,2,3,4,5,6 \\ 2 & \text{for } n = 7,8,9,10,11,12 \\ 3 & \text{for } n = 13,14,15,16,17,18 \end{cases} \tag{A-3}$$

$$q = \begin{cases} 1 & \text{for } \; n = 1,2,3,7,8,9,13,14,15 \\ 2 & \text{for } \; n = 4,5,6,10,11,12,16,17,18 \end{cases}$$
$$p = \begin{cases} 3 & \text{for } \; n = 1,2,3,7,8,9,13,14,15 \\ 4 & \text{for } \; n = 4,5,6,10,11,12,16,17,18 \end{cases} \tag{A-4}$$

$$f_1 = \frac{1}{4}(2 - 3\eta + \eta^3) \qquad f_2 = \frac{1}{4}(2 + 3\eta - \eta^3)$$
$$f_3 = \frac{L_z}{4}(1 - \eta - \eta^2 + \eta^3) \quad f_4 = \frac{L_z}{4}(-1 - \eta + \eta^2 + \eta^3) \qquad \eta = \frac{z}{L_z} \tag{A-5}$$

$$g'_i = \frac{\partial g_i}{\partial x} \text{ and } h^*_j = \frac{\partial h_j}{\partial y} \tag{A-6}$$

The matrix $[B]$ in Eqs. (15) and (16) is

$$[B] = [\underline{B}_1 \;\; \underline{B}_2 \;\; \cdots \;\; \underline{B}_n \;\; \cdots \;\; \underline{B}_{18}] \tag{A-7}$$

$$[\underline{B}_n] = \left[\begin{array}{c:c:c:c:c:c}
g_i' h_j f_q & 0 & -g_i'' h_j f_p & \frac{D_{66}}{\Delta} g_i' h_j f_p & -\frac{D_{56}}{\Delta} g_i' h_j f_p & 0 \\ \hdashline
0 & g_i h_j^* f_q & -g_i h_j^{**} f_p & -\frac{D_{56}}{\Delta} g_i h_j^* f_p & \frac{D_{55}}{\Delta} g_i h_j^* f_p & 0 \\ \hdashline
\begin{matrix} -\frac{D_{13}}{D_{33}} g_i' h_j \widehat{f}_p \\ -\frac{D_{34}}{D_{33}} g_i h_j^* \widehat{f}_p \end{matrix} & \begin{matrix} -\frac{D_{34}}{D_{33}} g_i' h_j \widehat{f}_p \\ -\frac{D_{23}}{D_{33}} g_i h_j^* \widehat{f}_p \end{matrix} & g_i h_j \widehat{f}_q & 0 & 0 & \frac{1}{D_{33}} g_i h_j \widehat{f}_p \\ \hdashline
g_i h_j^* f_q & g_i' h_j f_q & -2 g_i' h_j^* f_q & \begin{matrix} \frac{D_{66}}{\Delta} g_i h_j^* f_p \\ -\frac{D_{56}}{\Delta} g_i' h_j f_p \end{matrix} & \begin{matrix} -\frac{D_{56}}{\Delta} g_i h_j^* f_p \\ +\frac{D_{55}}{\Delta} g_i' h_j f_p \end{matrix} & 0 \\ \hdashline
\begin{matrix} g_i h_j \widehat{f}_q \\ -\frac{D_{13}}{D_{33}} g_i'' h_j \widehat{f}_p \\ -\frac{D_{34}}{D_{33}} g_i' h_j^* \widehat{f}_p \end{matrix} & \begin{matrix} -\frac{D_{34}}{D_{33}} g_i'' h_j \widehat{f}_p \\ -\frac{D_{23}}{D_{33}} g_i' h_j^* f_p \end{matrix} & \begin{matrix} -g_i' h_j \widehat{f}_p \\ +g_i' h_j f_q \end{matrix} & \frac{D_{66}}{\Delta} g_i h_j \widehat{f}_p & -\frac{D_{56}}{\Delta} g_i h_j \widehat{f}_p & \frac{1}{D_{33}} g_i' h_j f_p \\ \hdashline
\begin{matrix} -\frac{D_{13}}{D_{33}} g_i' h_j^* f_p \\ -\frac{D_{34}}{D_{33}} g_i' h_j^{**} f_p \end{matrix} & \begin{matrix} g_i h_j \widehat{f}_q \\ -\frac{D_{34}}{D_{33}} g_i' h_j^* f_p \\ -\frac{D_{23}}{D_{33}} g_i' h_j^{**} f_p \end{matrix} & \begin{matrix} -g_i' h_j^* \widehat{f}_p \\ +g_i h_j^* f_q \end{matrix} & -\frac{D_{56}}{\Delta} g_i h_j \widehat{f}_p & \frac{D_{55}}{\Delta} g_i h_j \widehat{f}_p & \frac{1}{D_{33}} g_i h_j^* f_p
\end{array}\right] \tag{A-8}$$

Here

$$g_i'' = \frac{\partial^2 g_i}{\partial x^2}, \quad h_j^{**} = \frac{\partial^2 h_j}{\partial y^2}, \quad \widehat{f}_q = \frac{\partial f_q}{\partial z}, \text{ and } \widehat{f}_p = \frac{\partial f_p}{\partial z} \tag{A-9}$$

The shape function matrix $[N]$ for a transition element is given by Eq. (A-1) where

$$[\underline{N}_n] = \left[\begin{array}{c:c:c}
g_i h_j f_q & 0 & 0 \\ \hdashline
0 & g_i h_j f_q & 0 \\ \hdashline
0 & 0 & g_i h_j f_q
\end{array}\right] \tag{A-10}$$

when 1, 2, 3, 7, 8, 9, 13, 14, 15 and

$$[\underline{N}_n]=\left[\begin{array}{c|c|c|c|c|c}
g_i h_j f_q & 0 & -g_i' h_j f_p & \dfrac{D_{66}}{\Delta} g_i h_j f_p & -\dfrac{D_{56}}{\Delta} g_i h_j f_p & 0 \\ \hline
0 & g_i h_j f_q & -g_i h_j^* f_p & -\dfrac{D_{56}}{\Delta} g_i h_j f_p & \dfrac{D_{55}}{\Delta} g_i h_j f_p & 0 \\ \hline
\begin{array}{c} -\dfrac{D_{13}}{D_{33}} g_i' h_j f_p \\ -\dfrac{D_{34}}{D_{33}} g_i h_j^* f_p \end{array} & \begin{array}{c} -\dfrac{D_{34}}{D_{33}} g_i' h_j f_p \\ -\dfrac{D_{23}}{D_{33}} g_i h_j^* f_p \end{array} & g_i h_j f_q & 0 & 0 & \dfrac{1}{D_{33}} g_i h_j f_p
\end{array}\right] \tag{A-11}$$

when n=4, 5, 6, 10, 11, 12, 16, 17, 18. i, j, p are q defined in Eqs. (A-3) and (A-4). Here

$$f_1=\frac{1}{4}(1-2\eta+\eta^2) \quad f_2=\frac{1}{4}(3+2\eta-\eta^2) \quad f_3=\frac{h}{2}(-1+\eta^2) \tag{A-12}$$

The shape function matrix $[N]$ for a displacement model is given by Eq. (A-1) where $[\underline{N}_n]$ is defined in Eq. (A-10) for all n.

References

Abbas, H., Gupta, N. K., and Alam, M. (2004), "Nonlinear response of concrete beams and plates under impact loading", *Int. J. Impact. Eng.*, **30**, 1039-1053.

Al-Taan, S. A. and Ezzadeen, N. A. (1995), "Flexural analysis of reinforced fibrous concrete members using the finite element method", *Comput. Struct.*, **56**(6), 1065-1072.

Bhatt, P. and Kader, M. A. (1998), "Prediction of shear strength of reinforced concrete beams by nonlinear finite element analysis", *Comput. Struct.*, **68**, 139-155.

Cerioni, R. and Mingardi, L. (1996), "Nonlinear analysis of reinforced concrete foundation plates", *Comput. Struct.*, **61**(1), 87-107.

Ferreira, A. J. M., Camanho, P. P., Marques, A. T., and Fernandes, A. A. (2001), "Modeling of concrete beams reinforced with FRP re-bars", *Comput. Struct.*, **53**, 107-116.

Gibson, R.F. (1994), *Principles of Composite Material Mechanics*, McGraw-Hill.

Hahn, H.T. and Tsai, S.W. (1973), "Nonlinear elastic behavior of unidirectional composite laminae", *J. Compos. Mater.*, **7**, 102-118.

Hu, H.T., Lin, F-M., and Jan, Y-Y. (2004), "Nonlinear finite element analysis of reinforced concrete beams strengthened by fiber-reinforced plastics", *Comput. Struct.*, **63**, 271-281.

Hu, H. T. and Schnobrich, W. C. (1990), "Nonlinear analysis of cracked reinforced concrete", *ACI Struct. J.*, **87**(2), 199-207.

Jiang, J. and Mirza, F. A. (1997), "Nonlinear analysis of reinforced concrete slabs by a discrete finite element approach", *Comput. Struct.*, **65**(4), 585-592.

Kwak, H. G. and Filippou, F. C. (1997), "Nonlinear FE analysis of R/C structures under monotonic loads", *Comput. Struct.*, **65**(1), 1-16.

Kwak, H. G. and Kim, S. P. (2002), "Nonlinear analysis of RC beams based on moment-curvature relation", *Comput. Struct.*, **80**, 615-628.

Nitereka, C. and Neale, K.W. (1999), "Analysis of reinforced concrete beams strengthened in flexure with composite laminates", *Can. J. Civ. Eng.*, **26**, 646-654.

Phuvoravan, K. and Sotelino, D. (2005), "Nonlinear finite element for reinforced concrete slabs", *J. Struct. Eng.*, **131**(4), 643-649.

Polak, M. A. and Vecchio F. J. (1993), "Nonlinear analysis of reinforced concrete shell", *J. Struct. Eng.*, **119**(12), 3439-3462.

Ramtekkar, G. S., Desai, Y. M. and Shah, A. H. (2002), “Mixed finite element model for thick composite laminated plates”, *Mech. Adv. Mater. Struct.*, **9**, 133-156.

Ramtekkar, G. S., Desai, Y. M. and Shah, A.H. (2004). “First-ply failure of laminated composite plates – A mixed finite element approach”, *J. Reinf. Plast. Compos*, **23**(3), 291-315.

Rattanawangcharoen, N. (2005), “First-ply failure analysis of laminated composite cylindrical panels”, *J. Reinf. Plast. Compos*, **24**(14), 1521-1537.

Rattanawangcharoen, N. (2006), “An analysis of weakly bonded laminated cylindrical panels”, *J. Reinf. Plast. Compos*, **25**(15), 1611-1628.

Saenz, L. P. (1964), “Discussion of ‘Equation for the stress-strain curve of concrete’ by Desayi, P. and Krishnan, S”, *ACI J.*, **61**(9), 1229-1235.

Shahawy, M. A., Arockiasamy, M., Beitelman, T., and Sowrirajan, R. (1996), “Reinforced concrete rectangular beams strengthened with CFRP laminates”, *Compos: Part B*, **27B**, 225-233.

Supaviriyakit, T., Pornpongsaroj, P., and Pimanmas, A. (2004), “Finite element analysis of FRP-strengthened RC beams”, *Songklanakarin J. Sci. Tech.*, **26**(4), 497-507.

Vecchio, F. J. (1989), “Nonlinear finite element analysis of reinforced concrete membranes”, *ACI Struct. J.*, **86**(1), 26-35.

CM